Systematic investigation of the structure of the Si(553)-Au surface from first principles

Sampsa Riikonen*
Departamento de Física de Materiales, Facultad de Química, Universidad del País Vasco (UPV/EHU), Apartado 1072, 20080 San Sebastián, Spain
and Donostia International Physics Center (DIPC), Paseo Manuel de Lardizabal 4, 20018 San Sebastián, Spain

Daniel Sánchez-Portal†
Centro de Física de Materiales, Centro Mixto CSIC-UPV/EHU, Apartado 1072, 20080 San Sebastián, Spain
and Donostia International Physics Center (DIPC), Paseo Manuel de Lardizabal 4, 20018 San Sebastián, Spain
(Received 10 December 2007; published 17 April 2008)

We present here a comprehensive search for the structure of the Si(553)-Au reconstruction. More than 200 different trial structures have been studied using first-principles density-functional calculations with the SIESTA code. An iterative procedure, with a step-by-step increase in the accuracy and computational cost of the calculations, was used to allow for the study of this large number of configurations. We have considered reconstructions restricted to the topmost bilayer and studied two types: (i) "flat" surface-bilayer models, where atoms at the topmost bilayer present different coordinations and registries with the underlying bulk, and (ii) nine different models based on the substitution of a silicon atom by a gold atom in different positions of a π-bonded chain reconstruction of the Si(553) surface. We have developed a compact notation that allows us to label and identify all these structures. This is very useful for the automatic generation of trial geometries and for counting the number of inequivalent structures, i.e., structures that have different bonding topologies. The most stable models are those that exhibit a honeycomb-chain structure at the step edge. One of our models (model "f2") reproduces the main features of the room temperature photoemission and scanning-tunneling microscopy data. Thus, we conclude that this model is a good candidate for the high temperature structure of the Si(553)-Au surface.

DOI: 10.1103/PhysRevB.77.165418 PACS number(s): 73.20.At, 71.15.Mb, 79.60.Jv, 68.35.B−

I. INTRODUCTION

During the past few decades, several complex surface reconstructions that exhibit one-dimensional metal wires have been extensively studied. The interest in these systems has been driven mainly by the theoretical prediction that the behavior of a one-dimensional metal should sensibly deviate from the Fermi liquid picture due to electron correlation.[1] However, the coupling between electrons and lattice vibrations is also enhanced in one dimension, and these systems present a strong tendency to suffer structural transitions that reduce their symmetry and destroy their metallicity. The competition between the effects of electron-electron and electron-phonon interactions makes the physics of one-dimensional systems quite a rich and interesting topic. In this context, the quasi-one-dimensional reconstructions formed by several metals on flat and vicinal Si(111) surfaces have been regarded as ideal systems to realize a one-dimensional metal. On the one hand, the existence of an electronic gap in the substrate allows for the existence of purely one-dimensional electronic states near the Fermi energy, which are associated with the metal chains in the surface. On the other hand, it was believed that, in some cases, the rigidity of the substrate could allow for the observation of characteristic features of the Tomonaga–Luttinger liquid in the photoemission experiments,[1,2] which avoids the appearance of broken-symmetry phases at sufficiently low temperatures. Furthermore, ordered arrays of well aligned wires can be formed over large areas on these substrates, which allow for accurate measurements using angle resolved photoemission spectroscopy (ARPES). In the case of vicinal substrates, the average terrace width can be controlled by the miscut angle, which provides a route to tuning interwire distances and interactions.[3]

Some examples of quasi-one-dimensional reconstructions that have attracted much attention in recent years are the Si(111)-(5×2)-Au,[3–7] Si(557)-Au,[8–16] Si(553)-Au,[17–24] and Si(111)-(4×2)-In (Refs. 25–37) surfaces. All of these systems clearly show one-dimensional features in ARPES and scanning-tunneling microscopy (STM) experiments. At least in the cases of the Si(557)-Au, Si(553)-Au, and Si(111)-(4×2)-In surfaces, some of these one-dimensional bands seem to be metallic at room temperature. However, these three reconstructions suffer structural distortions associated with metal-insulator transitions when the temperature is lowered.[12,21,24,25,29,30]

The photoemission spectrum of the Si(557)-Au surface is dominated by two proximal one-dimensional bands with paraboliclike dispersions. According to *ab initio* calculations based on the existing structural model,[10,11] these two bands are due to the spin-orbit splitting of a band coming from the hybridization of the states of the gold chains with their silicon neighbors.[13,38] These bands are half filled and exhibit, as the temperature is lowered, a metal-insulator transition that is accompanied by a periodicity doubling along the steps in the STM images.[12–14,16]

The Si(553)-Au surface, which has a smaller terrace width, shows two bands similar to those observed in the case of the Si(557)-Au system. It also shows a strongly dispersing one-dimensional band with a fractional $(\sim1/3)$ filling.[3,17] It was proposed that this one-third-filled band could provide the appropriate conditions to observe large spin-charge sepa-

ration. This is in contrast to half-filled bands, which are unstable against a Mott–Hubbard transition for large values of the electron-electron interaction, which prevents the observation of a Luttinger metal.[3] Unfortunately, the Si(553)-Au surface also undergoes a metal-insulator transition at low temperatures. The Si(553)-Au surface exhibits two Peierls-type distortions with $\times 2$ and $\times 3$ increases in the unit cell of the chains along the steps. This is consistent with the occupations of the bands mentioned above. Furthermore, the $\times 3$ periodicity seems to be associated with the step edge, while the $\times 2$ periodicity appears in the middle of the terraces. This is consistent with the origin of the half-filled bands in the gold wires. *Ab initio* calculations indicate that the gold atoms prefer to occupy silicon substitutional positions in the middle of the terraces.[9,11,18]

A good structural model is necessary to understand the physics of this system in detail. However, in contrast to the case of the Si(557)-Au surface, the structure of the Si(553)-Au reconstruction is not well established. Recently, Ghose *et al.*[19] proposed a structure based on the analysis of x-ray diffraction measurements. This model contains a double row of Au atoms decorating the step edge. This seems inconsistent with the experimental gold coverage and the model has proven to be unstable.[22] In a recent work,[18] we studied, using first-principles density-functional calculations, five different structural models based on an analogy with the structure of the Si(557)-Au surface and an earlier proposal by Crain *et al.*[3] using a single gold chain. The most stable structures were those in which the step edge is formed by a honeycomb chain (HC).[39]

In the present paper, we perform a more comprehensive search of the structure of the Si(553)-Au reconstruction. We have considered models in which the topmost bilayer contains eight atoms per 5×1 unit cell, including one gold atom. These models also take into account all different coordinations and registries with the underlying bulk. We refer to these models as "flat" surface-bilayer structures, and we have found that there are 210 inequivalent structures of this type when reasonable physical constraints are applied. These structures are automatically generated and an iterative procedure, with a step-by-step increase in the accuracy and computational cost of the calculations, is used to study this large number of configurations. We have also considered nine different structures that are obtained by the substitution of a silicon atom by a gold atom in different positions of a π-bonded chain reconstruction of the Si(553) surface.

As we will see, our most stable structures belong to the set of flat-bilayer models and exhibit a honeycomb-chain structure in the step edge. This is in agreement with the observation in our previous study. Indeed, the two most stable structures (labeled "f2" and "f4" models) correspond to structures that have already been explored in Ref. 18. This confirms that the analogy with the Si(557)-Au surface provides a good route to studying the structure of the Si(553)-Au reconstruction and, most probably, other related surfaces.[40] The simulated STM images of the f2 and f4 models are in good agreement with the available experimental data.[24,41] Their band structures also reproduce the main features of the photoemission data.[17,21] In particular, the band structure of the f2 model shows two dispersive one-dimensional bands and one of them, which is associated with a silicon dangling bond in the surface, has a small fractional occupation that is in agreement with the measurements. Therefore, we conclude that the f2 model is a good candidate for the structure of the Si(553)-Au.

Finally, we have developed a compact notation that allows us to label and identify all of the structures. This notation is instrumental to the automatic generation of trial geometries and for counting the number of inequivalent (having different bonding topologies) structures. This notation is applicable to other similar surfaces and we think that it will be useful to other similar structural investigations.

II. METHODS

A. Density functional calculations

Most of the calculations were performed using the SIESTA code.[42,43] We used the local density approximation[44] and norm conserving pseudopotentials.[45] The gold pseudopotential included scalar relativistic effects and was similar to that used in Ref. 46 and in our previous calculations.[7,16,18,22] Different basis sets were used for the silicon atoms (see below for more details). For the fastest calculation, a single-ζ (SZ) basis of numerical atomic orbitals[43,47,48] was used. The SZ basis uses only one radial function to represent the orbitals in the $3s$ shell and another one for the $3p$ shell. For more accurate calculations, a double-ζ (DZ) basis, which has two different radial functions for each angular momentum, and a double-ζ polarized (DZP) basis, which includes an additional polarization $3d$ shell, were used. For gold, a DZP basis was always used with two different radial functions to represent the $6s$ and $5d$ orbitals and a polarization $6p$ shell. The radius of the Si orbitals was 5.25 Bohr for those in the $3s$ shell and was 6.43 Bohr for those in the $3p$ and $3d$ shells. For Au, the radii of the $6s$ and $6p$ orbitals were 6.24 and 4.51 Bohr for the orbitals in the $5d$ shell.

We modeled the surface by using slabs with different thicknesses (depending on the desired accuracy). For the initial and fastest simulations, we used a slab containing only two silicon bilayers, whereas four bilayers were used to more accurately explore the energetics of the most favorable structural models. The atoms in the bottom silicon layer were kept at their ideal bulk positions and saturated with hydrogen atoms. A vacuum gap of 15 Å between neighboring slabs was used. To avoid artificial stresses, the lateral lattice parameter was always fixed to the bulk theoretical value that was calculated with similar approximations. The lattice parameter strongly depends on the basis set used. The calculated values are 5.53, 5.48, and 5.42 Å for SZ, DZ, and DZP basis sets, respectively. Therefore, it is necessary to rescale the coordinates when the result of a relaxation using a simple basis set is used as the initial guess for a calculation with a more complete basis. Systems were relaxed until the maximum force component along any direction was less than 0.04 eV/Å. Different Monkhorst–Pack[49] samplings of the surface Brillouin zone were utilized. In this paper, they will be referred to as $M_k \times N_k$, where M_k refers to the direction parallel to the step edge and N_k refers to the direction perpendicular to the step edge. A real-space grid equivalent to a

100 Ry plane-wave cutoff was used. The simulated STM images were obtained by using the Tersoff–Hamann theory[50] and the DZP basis set.

For the most stable systems, we also performed calculations using the VASP code.[51,52] Projected-augmented-wave potentials and a well converged plane-wave basis set with a cutoff of 312 eV were used. All of the structures were relaxed (the equilibrium lattice parameter of bulk silicon that was obtained with VASP was 5.41 Å).

B. Strategy of the structural search

Searching for the lowest-energy configuration of any surface reconstruction is a formidable task. Any trial geometry that is not completely absurd relaxes to a nearby local minimum. One can then manually generate additional configurations from the most favorable ones by using different physical (electron counting, coordination, etc.) arguments, hoping to eventually end up in the global minimum. However, the number of local minima scales roughly exponentially with the number of atoms involved in the reconstruction and the problem becomes intractable for large cells. Apart from this heuristic approach, one can use more sophisticated algorithms that can automatically find optimum geometries. Some examples are simulated annealing[53,54] and Monte Carlo simulations of different types, including genetic algorithms.[55–57] Monte Carlo techniques have been traditionally used to find cluster geometries[58] and have been recently extended to find surface reconstructions.[59,60] Unfortunately, these methods are computationally very expensive and require long simulations with thousands of evaluations of the system energy (and interatomic forces in some cases). In particular, genetic algorithms are very powerful but typically need hundreds of generations, in which each one contains tens of trial geometries.[58] Therefore, they are mostly restricted to the use of empirical interatomic potentials which, however, might not be sufficiently accurate to reproduce the energetics of the different geometries explored. The results can be further refined by calculating some of the most energetically favorable structures using *ab initio* methods. This approach has been adopted, for example, in Ref. 61 to study the Si(114) surface and in Ref. 62 to study the structure of Au_n clusters, where $n=38$, 55, and 75.

In the present work, we adopt a compromise between these two ideas. Due to the lack of reliable empirical potentials to represent the interaction between the gold and silicon atoms in the surface, we need to explore the energetics of the different models of the Si(553)-Au reconstruction at the density-functional theory (DFT) or similar level of theory. This precludes the use of Monte Carlo algorithms to perform a global search for the reconstruction structure. However, we do not want to restrict our search to explore a "few" structural models. Thus, we would rather make a *systematic* search of the optimum surface model within a large family of physically motivated structures. Our approach is as follows:

(i) a family of likely structural models for the Si(553)-Au surface reconstruction is defined by using a heuristic procedure based on the analogy with other related and better known surfaces;

(ii) a compact notation is designed to unambiguously label each of the possible structures within this family;

(iii) from each one of these labels, a trial geometry is automatically generated and an initial constrained relaxation is performed to avoid the appearance of unphysical bond distances;

(iv) "fast" density-functional calculations using SIESTA are used to relax each of the structures to its closest local energy minimum;

(v) the most stable configurations from step (iv) are studied by using more time consuming "accurate" SIESTA calculations;

(vi) finally, since the energy differences between different structural models are quite small, we check the energy ordering of the most stable configurations by using a different methodology: plane-wave calculations using the VASP code.

By "fast" SIESTA calculations we mean here calculations performed by using small basis sets (i.e., with a small number of basis orbitals per atom, such as SZ or DZ basis sets[42,43]), limiting the number of k points and optimized degrees of freedom, and/or using criteria that are less stringent than usual for the convergence of the self-consistency cycles. These approximations substantially reduce the computational cost. Therefore, it becomes possible to relax the hundreds of different configurations within our family of structures. We will see below that the energies obtained in this first step are reliable enough to select a set of a few tens of structures containing the most promising structural candidates. Accurate SIESTA calculations are performed for these configurations by using DZP basis sets, a larger k sampling, and well converged self-consistency. We can see that the use of a code that utilizes basis sets of atomic orbitals is instrumental for this gradual increment of the accuracy of the calculations: while the pseudopotentials, density functional, and basic numerical scheme remain unchanged, the size of the basis set (the main factor limiting the size of the studied systems and the computational time) can be varied. This provides a very convenient way of dealing with the trade-off between computational speed and accuracy of the calculation. For Si(111)-(5×2)-Au, we have recently shown that SIESTA calculations using DZP basis sets are in excellent agreement with well converged plane-wave calculations.[7] In the present work, we confirm this observation for the proposed models for the Si(553)-Au surface. This seems to confirm that our final structures are the most favorable within the family of structures considered here.

In the following, we present the hierarchy of approximations used to perform our simulations in detail. As a starting point, we automatically generate approximate coordinates for all possible structures fulfilling certain conditions. These conditions will be explained in detail in the next section. Our family of structural models is based on plausible analogies with the structure of other related surface reconstructions such as Si(557)-Au or Si(111)-(5×2)-Au. While reasonable atomic coordinates within the plane of the terrace (that we take as the xy plane) are relatively easy to guess due to the registry with the subsurface bilayer, the height of the different atoms in the surface bilayer is more problematic. For this reason, in the first relaxation (named Sz hereafter), only the

atoms in the topmost bilayer are allowed to relax in the z direction (normal to the terrace). This relaxation step ensures that the interatomic distances become reasonable without changing the topology of the surface bilayer and its registry with the underlying atoms. For the *Sz* relaxations, we use a SZ basis set and a 2×1 k sampling. To further accelerate the simulations, the parameter determining the convergence of the density matrix in each relaxation step (DM. Tolerance[63]) is set to 10^{-3}. The typical value given to this parameter to ensure a very good convergence of the self-consistent solution is 10^{-4}. However, we have checked that increasing this value to 10^{-3} only introduces small errors in the calculation of energy and forces: for example, the maximum force difference during the relaxation of a few representative structures of those studied here was less than 0.01 eV/Å when the two different convergence criteria were used. In spite of this moderate effect on the results, in some cases, increasing the value of DM. Tolerance to 10^{-3} considerably reduces the number of iterations per self-consistency cycle. In the next step (named *Sy* hereafter), all atoms are allowed to move (except the silicon atoms in the bottom of the slab and the hydrogen atoms directly bonded to them). However, in order to preserve the topology of the selected configuration, the positions of the atoms along the direction parallel to the step edges (y axis) is fixed. Other parameters have the same value as in the relaxation *Sz*. The purpose of the relaxations *Sz* and *Sy* is to provide a sound initial configuration from the automatically generated coordinates. By using this corrected guess, we proceed to relax all the degrees of freedom in the slab with a more complete DZ basis set and an accurate 8×4 k sampling. We call this the $D^{\star}$ relaxation. Finally, in the *D* relaxations, we further decrease the tolerance for the convergence of the elements of the density matrix to its usual default value in SIESTA (Ref. 63) of 10^{-4}. We use a DZP basis set for our most accurate relaxations (*DP* hereafter). Adding a polarization shell with d symmetry can be especially important to accurately describe "unusual" coordinations of the silicon atoms that cannot be described with simple *sp* hybridizations.

The use of this series of optimization schemes with ever-increasing accuracy ($Sz\rightarrow Sy\rightarrow D^{\star}\rightarrow D\rightarrow DP$) is much more efficient than directly starting with a relaxation at the *DP* or similar level. The reason for this efficiency gain is twofold: (i) the initial coordinates used to start each relaxation have been optimized at the previous level and, therefore, they are an initial guess of increasing quality; (ii) the energy estimates obtained with less accurate relaxations, which are already at the *Sy* level, are accurate enough to allow excluding many of the less favorable models. One has to take into account the fact that a minimal basis for Si contains only four orbitals, a DZ basis has eight orbitals, and a DZP basis has 13 orbitals. Thus, the computational cost dramatically changes when the basis set size is changed. Additional gains are obtained by using a smaller k-point sampling and reducing the number of steps in each self-consistency cycle.

C. Structural models: A labeling scheme

The structural models that we considered here for the Si(553)-Au reconstruction are based on analogy with other similar reconstructions,[3] for which there are more structural data. In particular, the vicinal Si(557)-Au surface reconstruction has been extensively studied in recent years, and its structure has been established from x-ray studies[10] and DFT calculations.[9,11,13] Similar to the case of the Si(553)-Au surface, the steps of Si(557)-Au run along the $[\bar{1}10]$ direction and each terrace contains a monatomic chain of gold atoms. However, while for Si(553)-Au the surface normal is tilted from the [111] direction toward the $[11\bar{2}]$ direction, the normal to the Si(557)-Au surface is tilted toward the opposite direction ($[\bar{1}\bar{1}2]$).[3] The size of the terraces is also different; it is larger in the case of Si(557)-Au, which allows for the presence of a row of silicon adatoms running parallel to the step edge[10,11] that seems to be absent in the case of the Si(553)-Au surface. Therefore, it is clear that both structures can be quite different (particularly the step-edge configuration), and one has to be careful when trying to translate structural information from one system to the other.

Fortunately, we also have a considerable amount of information about the reconstruction induced by submonolayer deposition of gold in flat Si(111). The structure of the Si(111)-(5×2)-Au surface, which corresponds to a larger gold coverage than those commented above, was experimentally established by Marks and Plass[64] using high resolution electron microscopy and heavy-atom holography. Recent first-principles calculations have shown that the real structure is probably somewhat different from this original proposal[5,7,65] and might even depend on the concentration of silicon adatoms present in the surface.[7,66] However, there are several elements common to most of the proposed models, which are also shared by the Si(557)-Au reconstruction. The most important features of the most stable structural models of these surfaces are as follows:

(i) the reconstruction only involves the atoms in the topmost bilayer;
(ii) the gold atoms occupy substitutional positions in the surface layer, which are much more favorable than adatom-like sites;
(iii) the positions of gold in the middle of terraces are favored over step-edge decoration; and,
(iv) the frequent appearance of the so-called honeycomb-chain[39] structure.

Figure 1(a) shows a schematic view of an unreconstructed Si(553) surface. Taking into account points (i) and (ii), here we only explore reconstructions that are generated by adding an additional bilayer on top of this unreconstructed substrate. One of the silicon positions is replaced by a gold atom. Different registries with the underlying bilayer as well as the presence of HC structures are allowed. Figures 1(b)–1(d) show a few possible structures. Figure 1(b) recovers the unreconstructed surface. Figure 1(c) presents a stacking fault (SF) in the middle of the terrace with the accompanying surface dislocations with under- and overcoordinated atoms (indicated by arrows in Fig. 1). In Fig. 1(d), the surface bilayer contains a HC structure in the middle of the terrace. Notice that the HC reconstruction also creates a stacking fault toward the $[\bar{1}\bar{1}2]$ direction (i.e., toward the inner part of

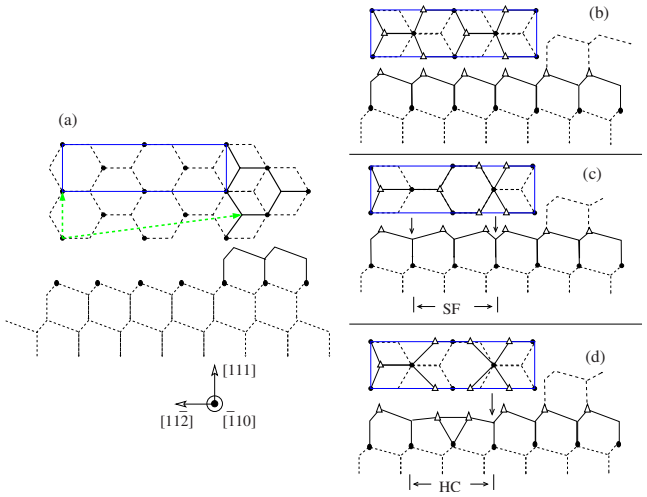

FIG. 1. (Color online) (a) Schematic view of the unreconstructed Si(553) surface. The steps run parallel to the $[\bar{1}10]$ direction and are oriented toward the $[11\bar{2}]$ direction. The rectangle indicates a "unit cell" *within* the terrace, which contains nine inequivalent silicon sites (with four unsaturated dangling bonds). The actual lattice vectors of the reconstruction are indicated by dashed arrows. The width of the terraces is $(4+1/3)\times\sqrt{3/8}a_{\mathrm{Si}}$ ($\sim$14.4 Å) with a_{Si} as the bulk lattice parameter of Si. (b)–(d) show the configurations generated by adding a silicon bilayer on top of the structure in (a). The different reconstructions explored in this paper are obtained by changing the structure of this surface bilayer and/or its registry with the underlying atoms. Open triangles represent the topmost atoms and solid circles the higher atoms in the second bilayer. These structures (and all of the structures considered in the present work) preserve a $\times 1$ periodicity along the step. Therefore, the size of the unit cell along the $[\bar{1}10]$ direction is always $1/\sqrt{2}a_{\mathrm{Si}}$ ($\sim$3.8 Å). Structure (b) recovers an unreconstructed silicon structure. Structure (c) presents a surface dislocation close to the step edge that generates a SF that is later corrected by creating another surface dislocation in order to connect with the bulk structure. Surface dislocations create under- and overcoordinated atoms, which are indicated by arrows. (d) presents a HC structure and the accompanying surface dislocation.

the terrace). This stacking fault has to be corrected in order to connect with the bulk structure. Therefore, it is necessary to introduce a surface dislocation with overcoordinated atoms (marked with an arrow). The role of this surface dislocation in relation to a nomenclature describing the models of the Si(553)-Au surface containing the HC structure was discussed in detail by Riikonen and Sánchez-Portal.[18]

The importance of the HC structure for the gold induced reconstructions on vicinal Si(111) was recently emphasized by Crain *et al.*[3] It is known to form the step edge of the Si(557)-Au surface.[9–11,16] It is also a key ingredient of the most recent proposals for the structure of the Si(111)-(5 $\times$2)-Au reconstruction.[5,7] The HC structure was initially proposed to explain the low coverage reconstructions induced by some alkali metals (Li, Na, and K), Mg, and Ag on Si(111).[39] We see that the HC structure involves two unit cells of the unreconstructed Si(111) surface, with one atom removed from the top Si layer. This flattens the surface and removes surface stress. The two silicon atoms in the center of the HC structure have a double bond, which is further stabilized by its hybridization with the dangling bond of the atom immediately below. In the case of reconstructions induced by alkalis, the metal atoms donate electrons to the HC, which becomes a closed-shell structure and, thus, contribute to the stabilization of the surface.[39] In the case of gold, which has a stronger electron affinity, the situation is different. Gold is likely to take electrons away from the silicon structure. In principle, this does not prevent an electronic stabilization mechanism: one electron may be transferred to the 6*s* Au state, leading again to a closed-shell structure. However, we are typically far from this *ionic* situation. The states of gold are strongly hybridized with those of the neighboring silicon atoms, which create several dispersive bands that are, in principle, metallic[9,11,13] and dominate the photoemission spectra.

In Ref. 18, we explored a few structural models for the Si(553)-Au reconstruction based on an analogy with the Si(557)-Au surface. Here, we want to move a step further and to make a comprehensive search among the structural models that can be built following rules (i)–(iv) presented above. We consider *all* possible structures where the atoms of the topmost bilayer present coordinations between 2 and 4 with other atoms in the same bilayer. The final coordination depends on the registry with the underlying silicon structure. One of the silicon atoms in the unit cell is replaced by a gold atom. The Si(553)-Au reconstruction is known to suffer several distortions that increase the size of the unit cell along the step direction as the temperature is decreased.[21,24] However, here, we only consider models that preserve the $\times 1$ periodicity of the silicon substrate along the steps and, therefore, are relevant to the model of a high temperature structure.

We have developed a simple labeling scheme for the family of structural models that fulfill the criteria presented above. We can label each structure and, thus, count the total number of different trial structures within this family. Furthermore, this scheme can easily be translated into a procedure for automatically generating the trial geometries. The basis of our labeling procedure can be found in Fig. 2. First, the possible positions within the *xy* plane of the surface atoms are discretized and approximated by the points of a grid. The grid is formed by nine columns and two rows. The nine columns correspond to the positions of the atoms along the $[11\bar{2}]$ direction in the terrace of an unreconstructed Si(553) surface [see Fig. 1(b)]. Second, all possible structures created by distributing the atoms among the grid points can be translated into a sequence of nine numbers. The position along the horizontal coordinate (column) is indicated by the order in the numerical sequence. The first number corresponds to the atoms at the step edge. For a given column, a "2" ("4") indicates that a silicon (gold) atom is located in the higher row, i.e., in the middle of the rectangular terrace unit cell, whereas a "1" ("3") indicates that a silicon (gold) atom sits over a grid point in the lower row. A "0" indicates that there are no atoms in that column. By using this scheme, the unreconstructed Si(553) surface in Fig. 1(b) can be labeled as (1,2,2,1,1,2,2,1,1), while structures in Figs. 1(c) and 1(d) would receive the labels (1,2,2,2,1,1,2,1,1) and (1,2,2,1,0,1,2,1,1), respectively. Other examples, which cor-

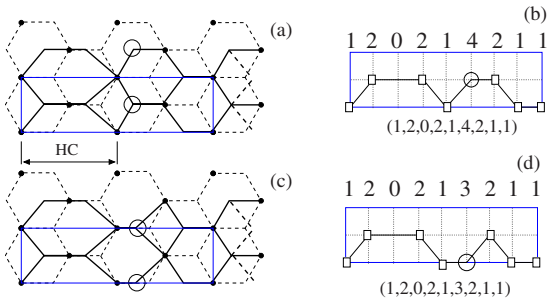

FIG. 2. (Color online) (a) and (c) show two possible structures for the Si(553)-Au surface already explored in Ref. 18. These structures are characterized by the presence of a HC structure close to the step edge. Solid lines indicate the bonds between atoms in the topmost bilayer of a given terrace, thin dashed lines correspond to the underlying silicon bilayer, and thick dashed lines indicate a few bonds of the upper terrace. The small solid circles mark the positions of the higher silicon atoms in the underlying bilayer. The large open circles mark the substitutional sites occupied by the gold atoms. The rectangles mark the terrace unit cell. (b) and (d) schematically explain how the structure of the surface bilayer can be translated into a sequence of nine numbers. First, the possible positions of the atoms are approximated by the points of a grid. The grid is formed by nine columns and two rows. The position along the horizontal coordinate is indicated by the order in the numerical sequence. The first number corresponds to the atoms at the step edge. A "2" ("4") indicates that a silicon (gold) atom is located in the higher row, i.e., in the middle of the rectangular cell. A "1" ("3") indicates that a silicon (gold) atom sits over a grid point in the lower row. A "0" indicates that there are no atoms in that column.

respond to models already studied in Ref. 18, can be found in Fig. 2.

In principle, by using our notation, we can generate M different models, with

$$M = 2^{(N_{\mathrm{Si}}+1)} \frac{9!}{(8-N_{\mathrm{Si}})!\,N_{\mathrm{Si}}!}, \tag{1}$$

where N_{Si} is the number of silicon atoms in the surface bilayer. Since we always have one gold atom, the total number of atoms in the terrace unit cell is $N_{\mathrm{atm}}=N_{\mathrm{Si}}+1$. Here, we consider structures with $N_{\mathrm{Si}}=7$. In this way, the family of structures studied here includes the five models already discussed in Ref. 18. Furthermore, having $N_{\mathrm{atm}}=8$ is a necessary condition to allow for the formation of the HC structure, which is one of the common building blocks to several gold induced reconstructions in Si(111) and vicinal Si(111) surfaces (see above). With $N_{\mathrm{Si}}=7$, we have $M=18\,432$ different models. This large number can be considerably reduced by imposing a few constraints to ensure that the models represent physically sound structures. These constraints are the following: (a) in order to connect with the bulk structure, the last number of the series must either be 1 or 3; (b) the dangling bonds of the underlying silicon bilayer must be saturated either by an atom or by a dimer as in the HC structure; therefore, the first number of the labeling sequence must always be 1 or 3; (c) the fifth number must be 0, 1, or 3 (if 0, then the neighboring numbers must either be 1 or 3); (d) the third and seventh numbers must be 0, 2, or 4 (if 0, then the neighboring numbers in the sequence must be 2 or 4); (e) to ensure the connectivity within the surface bilayer, a nonzero number in the sequence cannot be surrounded by zeros; and, (f) two or more zeros cannot appear together. By taking into account conditions (a)–(f), the number of possible configurations with $N_{\mathrm{atm}}=8$ and $N_{\mathrm{Si}}=7$ is reduced to $M=210$. In this work, we will explore these 210 configurations by using fast SIESTA calculations, as described in the previous section, and a few tens of the most stable configurations will be selected to perform more accurate SIESTA and VASP calculations.

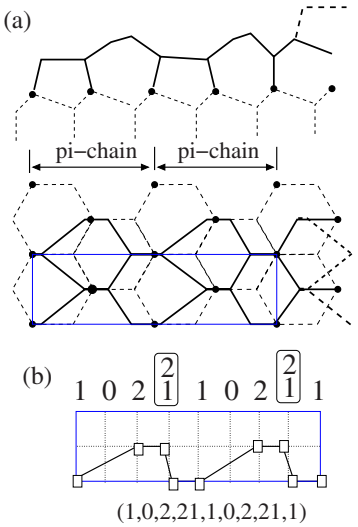

FIG. 3. (Color online) (a) Scheme of a π-bonded chain reconstruction of the Si(553) surface and (b) the proposed notation for such structure. The presence of the π-bonded chain at a certain location is indicated by the double occupation of the corresponding column; the second atom of this pair occupies the higher position along the π chain.

Our notation provides information about the connectivity within the surface bilayer and the registry with the substrate. From a given sequence of nine numbers, we can generate a trial geometry. However, we lack information about the heights of the different atoms. Because of this and the discretization of positions in the xy plane, the bond lengths and angles in the automatically generated structures can considerably depart from the correct values. For this reason, as a first step to get sound initial configurations, we need to perform constrained relaxations that, while preserving the bonding topology of the selected configuration, avoid unphysical bond distances and angles. For this purpose, we use the Sz and Sy relaxations described in the previous section.

Besides the family of structures described above, we have explored a few structural models based on the π-bonded chain reconstruction of the Si(111) surface.[67–69] In principle, our notation cannot describe these bonding patterns: it can only describe structures that are based on a flat surface bilayer. This is partially due to the lack of information about the atomic heights. However, we can modify our notation to describe the π-bonded chain structures. This is done by allowing a double occupation of the columns, which is schematically illustrated in Fig. 3. This double occupation indicates the position of the π-bonded chain in the structure. There is still ambiguity about the relative height of atoms in

the π-bonded chain, which is known to be tilted. There are two possibilities, which are usually referred to as a negative or a positive tilt.[70] In our notation, these two different tilts of the π chain are indicated by the order of the pair of indices, with the second index corresponding to the higher atom. In Fig. 3, we present a Si(553) surface reconstructed with the negative-tilt chain. This negative-tilt π-chain block corresponds to the label (…,1,0,2,21,1,…), while the label (…,1,0,2,12,1,…) denotes the positive-tilt structure. Both configurations are quite similar and first-principles calculations predict them to be almost degenerate in energy and separated by a very small energy barrier.[71,72] Experimentally, the positive-tilt structure has been traditionally favored.[68–70] In the case of the Si(553) stepped surface, our calculations predict the negative-tilt structure to be slightly more stable.

This notation opens the possibility of generating and studying all possible structures containing the π-bonded chain. However, we have not pursued this approach here and we limit ourselves to considering nine different structural models that are obtained after the substitution of one silicon atom by a gold atom in different positions of a π-bonded chain reconstruction, which is similar to that shown in Fig. 3.

III. RESULTS

We take advantage of the methodology described in Secs. II B and II C to make an extensive search of the structure of the Si(553)-Au reconstructions. We make a systematic search within the 210 structures that can be generated with the notation presented in Sec. II C (models based on flat bilayers with different coordinations and registries with the substrate) with seven silicon atoms and one gold atom in the terrace unit cell. We also present results from a much more restricted search for structures based on the π-bonded chain reconstruction. Finally, the most stable structures from these two searches are studied by using accurate SIESTA and VASP calculations. We present results for the band structure and the simulated STM images of some of the final models.

A. Systematic search: Flat bilayers with $N_{atm}=8$

We first explore the energy of the 210 possible configurations by using our fastest relaxation schemes, *Sz* and *Sy*, which were described in Sec. II B. These calculations transform an initial structure that is automatically generated from a given label into a physically sound structure. In spite of the thin slab and the minimal basis utilized, the relative energies obtained at the *Sy* level (ΔE_1) already provide a good guide to eliminating the most unstable structures. In Table I, we can find a list with the 80 most stable configurations ($\Delta E_1 \leq 33$ meV/Å^2) obtained after *Sy* relaxations. Several of the initial structures converge to the same configuration, such that these 80 trial structures give rise to only 40 clearly different structures. This is seen in Fig. 5, where the plateaus in the energy curve correspond to this "lumping" of several initial geometries into a single geometry. This transformation typically takes place by a displacement of the surface bilayer as a whole, thus changing its registry with the underlying substrate, or by the movement of a vacancy to a neighboring

TABLE I. Results from the automatic structural search. Total energies ΔE_1 are obtained using a thin slab of only two silicon bilayers and the fastest (and less accurate) relaxations (*Sz* and *Sy*). Only the 80 most stable configurations (out of the 210 total studied structures) are included in this table, with a maximum energy difference of $\Delta E_1 \sim 33$ meV/Å^2. The configurations are numbered according to their predicted stability. The initial configurations are labeled using the notation developed in Sec. II C. The 68 most stable structures according to ΔE_1 are also calculated using a thicker slab of four bilayers and our accurate SIESTA calculations ($D^\star \rightarrow D \rightarrow DP$), resulting in ΔE_2 energy differences. Several initial configurations converge to a single structure. Some of the final structures are indicated with labels f1–f10 (see also Figs. 5 and 6).

No.	Initial configuration	ΔE_1 (meV/Å^2)	ΔE_2 (meV/Å^2)
1	1,2,2,0,1,1,4,1,1	0.00	0.00
2	1,2,2,1,0,1,4,1,1	0.00	0.00
3	1,2,2,1,1,0,4,1,1	0.00	0.00
4	1,2,0,2,1,1,4,1,1	0.00	0.00(f1)
5	1,0,2,2,1,1,4,1,1	0.01	−0.01
6	1,2,2,0,1,3,2,1,1	5.51	−4.27
7	1,2,2,1,0,3,2,1,1	5.51	−4.29
8	1,0,2,2,1,3,2,1,1	5.51	−4.26
9	1,2,2,1,3,0,2,1,1	5.53	−4.30
10	1,2,0,2,1,3,2,1,1	5.54	−4.28(f2)
11	1,2,2,1,1,0,2,3,1	6.08	−4.02
12	1,2,0,2,1,1,2,3,1	6.09	−4.01(f3)
13	1,2,2,0,1,1,2,3,1	6.09	−4.02
14	1,2,2,1,0,1,2,3,1	6.09	−4.01
15	1,0,2,2,1,1,2,3,1	6.12	−4.02
16	1,0,2,2,1,4,2,1,1	6.21	−4.42
17	1,2,0,2,1,4,2,1,1	6.23	−4.46(f4)
18	1,2,2,0,1,4,2,1,1	6.29	−4.45
19	1,2,0,2,3,2,2,1,1	7.47	1.75(f5)
20	1,2,2,0,3,2,2,1,1	7.49	1.73
21	1,0,2,2,3,2,2,1,1	7.49	1.74
22	1,0,4,1,1,2,2,1,1	14.69	9.55(f6)
23	1,2,2,1,1,0,2,4,1	14.76	−0.20
24	1,2,2,1,0,1,2,4,1	14.76	−0.20
25	1,2,2,1,1,2,0,4,1	14.77	−0.21
26	1,2,0,2,1,1,2,4,1	14.77	−0.17(f7)
27	1,2,2,0,1,1,2,4,1	14.78	−0.20
28	1,2,2,1,1,2,4,0,1	14.82	−0.18
29	1,0,2,2,1,1,2,4,1	15.41	−0.20
30	1,0,2,2,1,3,2,2,1	17.49	16.12
31	1,2,0,2,1,3,2,2,1	17.49	16.13
32	1,2,2,0,1,3,2,2,1	17.50	5.77
33	1,0,2,3,1,2,2,1,1	21.98	1.89
34	1,0,2,4,1,2,2,1,1	22.57	5.00
35	1,2,2,1,1,2,0,2,3	23.49	12.80
36	1,2,2,1,1,2,2,0,3	23.49	12.79
37	1,2,2,1,0,1,2,2,3	23.64	11.70

TABLE I. (*Continued.*)

No.	Initial configuration	ΔE_1 (meV/Å^2)	ΔE_2 (meV/Å^2)	
38	1,2,2,0,1,1,2,2,3	23.68	11.55	
39	1,2,2,1,1,0,2,2,3	23.72	12.78	
40	1,0,2,2,1,1,2,2,3	23.79	12.20	
41	1,2,2,0,3,1,2,1,1	23.88	7.47	
42	1,2,2,3,0,1,2,1,1	23.90	7.48	
43	1,2,2,3,1,0,2,1,1	23.91	7.47	
44	1,2,0,2,3,1,2,1,1	23.91	7.47	
45	1,0,2,2,3,1,2,1,1	23.91	7.47	
46	1,2,0,2,1,1,2,2,3	24.13	12.18	
47	1,2,0,2,1,2,4,1,1	25.23	7.76	
48	1,0,2,2,1,2,4,1,1	25.24	7.77	
49	1,2,2,0,1,2,4,1,1	25.24	7.77	
50	1,2,0,2,1,2,2,3,1	25.41	4.17	(f8)
51	1,2,2,0,1,2,2,3,1	25.41	4.13	
52	1,0,2,2,1,2,2,3,1	25.42	4.13	
53	1,2,0,4,1,2,2,1,1	25.67	11.56	
54	1,2,4,0,1,2,2,1,1	25.72	11.50	
55	1,4,2,0,1,1,2,1,1	26.31	9.40	
56	1,4,2,1,0,1,2,1,1	26.34	9.40	
57	1,4,2,1,1,0,2,1,1	26.36	9.40	(f9)
58	1,4,0,2,1,2,2,1,1	27.35	12.50	
59	1,0,4,2,1,2,2,1,1	27.35	12.49	
60	1,2,4,0,1,1,2,1,1	27.37	15.34	
61	1,4,2,0,1,2,2,1,1	27.40	12.50	
62	1,2,2,3,1,2,2,0,1	27.62	2.66	
63	1,2,2,3,1,2,0,2,1	27.63	2.66	(f10)
64	1,2,2,3,0,1,2,2,1	27.63	2.68	
65	1,4,2,1,1,0,2,2,1	28.08	11.52	
66	1,0,4,2,1,1,2,2,1	28.09	9.70	
67	1,4,2,1,0,1,2,2,1	28.09	9.75	
68	1,4,2,0,1,1,2,2,1	28.09	9.75	
69	1,2,2,1,0,3,2,2,1	28.91		
70	1,2,0,4,1,1,2,1,1	29.48		
71	1,2,4,1,0,1,2,1,1	29.48		
72	1,2,4,1,1,0,2,1,1	29.51		
73	1,0,2,1,1,4,2,1,1	32.35		
74	1,1,2,4,1,0,2,2,1	33.05		
75	1,1,2,4,1,2,2,0,1	33.05		
76	1,1,2,4,1,2,0,2,1	33.06		
77	1,2,0,2,3,1,2,2,1	33.43		
78	1,2,2,0,3,1,2,2,1	33.43		
79	1,0,2,2,3,1,2,2,1	33.43		
80	1,2,0,2,1,2,2,1,3	33.48		

position [by using our notation, this corresponds to a transformation $(\ldots,0,1,2,\ldots)\rightarrow(\ldots,1,0,2,\ldots)$]. This happens, for example, in the case of the (1,2,2,1,1,0,4,1,1) initial structure, which transforms into a configuration that is better described with the label (1,2,0,2,1,1,4,1,1) and is one of the most stable structures. This can be seen in Fig. 4 (see also Table I).

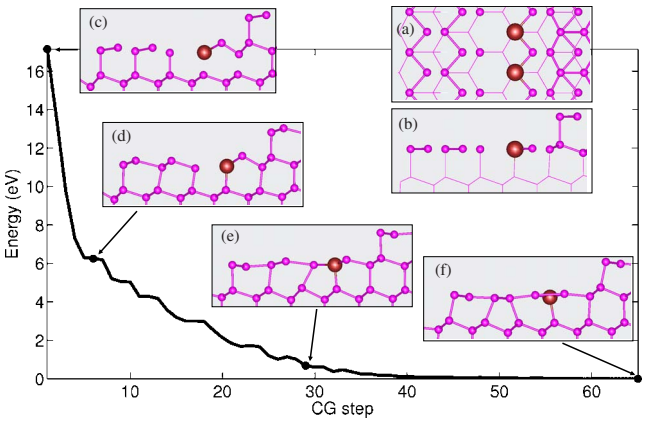

FIG. 4. (Color online) Relaxation of the structure generated from the label (1,2,2,1,1,0,4,1,1) at the *Sy* level. (a) and (b) present a top and a lateral view of the automatically generated structure. (c) presents the structure after the relative heights of the atoms have been corrected by the *Sz* relaxation. In (d), we have already reached a structure similar to the configuration that we want to explore. However, this configuration is not stable and transforms by the displacement of the surface bilayer (e) into a different structure. The final structure, shown in (f), is better described by the (1,2,0,2,1,1,4,1,1) label.

The 68 most stable structures, as predicted by using ΔE_1, are then calculated again, this time with more accurate relaxation schemes up to the *DP* level (for details, see Table I). Hereafter, we will refer to these final relative energies as ΔE_2 to the *DP* level. The comparison between ΔE_1 and ΔE_2 can be found in Table I and Fig. 5. Of course, there are important differences between the relative energies calculated by using the minimal basis and constrained relaxations (*Sy* scheme) and those obtained from the fully relaxed structures by using DZP basis sets (*DP* scheme). However, the overall trend of increasing energy is recovered with the more accurate calculations. We also observe in this case that several initial geometries give rise to the same or very similar final structures.

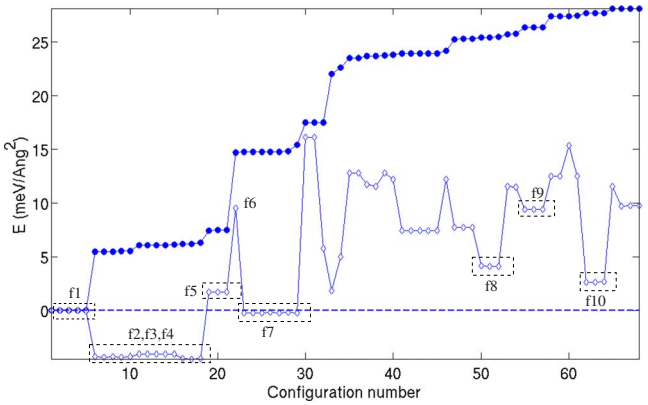

FIG. 5. (Color online) Relative energies after fast *Sy* (ΔE_1, solid circles) and accurate *DP* (ΔE_2, open diamonds) relaxations for the systems listed in Table I. The system labels f1–f10 correspond to those of Table I and Fig. 6.

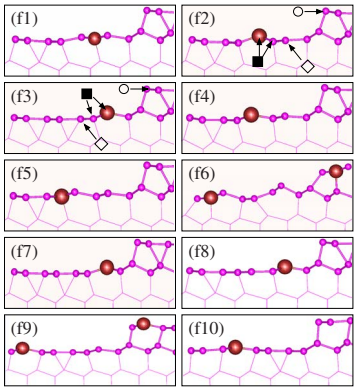

FIG. 6. (Color online) Final geometries (at the *DP* level) for a few selected configurations from those listed in Table I and Fig. 5. In the case of the f2 and f3 structures, some symbols are assigned to a few atoms in the surface. They will be used to indicate the main character of the different bands (see Fig. 7).

However, some of the approximate degeneracies found with the constrained relaxations are removed.

Some of the most stable final geometries are marked with labels f1–f10 in Fig. 5 and Table I. These structures are shown in Fig. 6. The fast *Sy* relaxations (ΔE_1) predicted f1 to be the most stable configuration. It exhibits a HC structure at the step edge, while the gold atom is located at a surface dislocation in the middle of the terrace. As discussed in Sec. II C, the presence of a surface dislocation is necessary to recover the bulk stacking disrupted by the HC. The position of the gold atom seems reasonable, in which gold should be a better option than silicon to sit at the dislocation since gold does not exhibit a strong directional bonding. However, by using a more complete basis set (already a DZ basis gives the correct result) and a thicker slab, the f2–f4 geometries become the most favorable structures (they are almost degenerate and ~ 4 meV/Å^2 more stable than f1). This points to the importance of using more complete (and, thus, flexible) basis sets when the coordination of the surface atoms departs from a simple *sp* hybridization (as in the case of the HC structure or at the surface dislocations).

Our results indicate that the configurations featuring a HC structure at the step edge [similar to the Si(557)-Au structure] are the most stable, at least within the family of reconstruction considered here. This confirms the results obtained in our previous work,[18] where we only studied six different models (one of them was the model proposed by Crain *et al.*,[3] which exhibits a $\times 3$ periodicity and, therefore, lies outside the present family of models). The configurations f4 and f2 in the present study correspond to the most stable structures obtained in Ref. 18 (named I and II, respectively, in that reference). Also configurations f8, f9, and f10 correspond to structures III, IV, and V in Ref. 18. Configuration f3, however, is a different configuration exhibiting a double honeycomb structure similar to that found in some models of the Si(111)-(5×2)-Au reconstruction.[5,7]

In Sec. II C, we pointed out that our labeling scheme excludes, in principle, structures based on the π-bonded chain reconstruction. However, in Fig. 6, we can find one structure where the π-bonded chain reconstruction has emerged spontaneously. In configuration f6, the gold atom is located very close to the step edge. The initial structure corresponds to a largely unreconstructed terrace. It is well known[73] that the energy barrier for the transformation from the unreconstructed Si(111) to the π-bonded chain Si(111)-(2×1) reconstruction is very small. Therefore, the appearance of the π-bonded chain in this case is not very surprising.

The experimental electronic band structure, as determined by photoemission expriments,[3,17,21] presents three bands with a parabolic dispersion and a strong one-dimensional character. Two of them are similar to those found for the Si(557)-Au surface and, therefore, can be assigned to the spin-split bands formed from the hybridization of Au 6*p* states with the *sp* lobes of the neighboring Si atoms, as proposed in our recent work.[13] The third band appears centered around the same point in reciprocal space, but at higher energies and thus has a lower occupation of around 1/3.

In Fig. 7, we can find the band structures of the models f2 and f3. The band structure of the model f4 has been published elsewhere.[18] The geometries of f2 and f4 are very similar (see Fig. 6) but their band structures present some small but essential differences. Both models present one dispersive one-dimensional band coming from the hybridization of gold with its silicon neighbors. This band can be identified with the spin-split bands observed in the Si(553)-Au surfaces[17,38] and Si(557)-Au.[8] Two other surface bands ap-

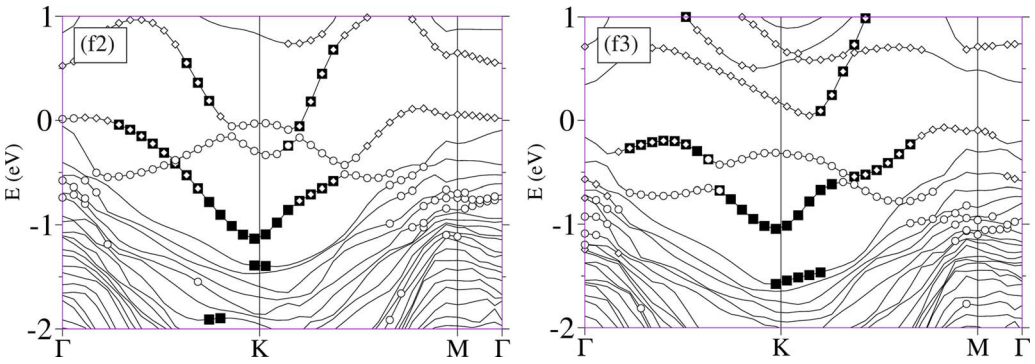

FIG. 7. (Color online) Band structures of models f2 and f3 as calculated by using SIESTA. The atomic character of the different bands is indicated by using the symbols in Fig. 6. Filled squares indicate the contribution coming from the gold atoms and their silicon neighbors, open circles indicate contribution coming from the atoms at the step edge, and open diamonds indicate that of some silicon atoms in the surface, which present unsaturated bonds.

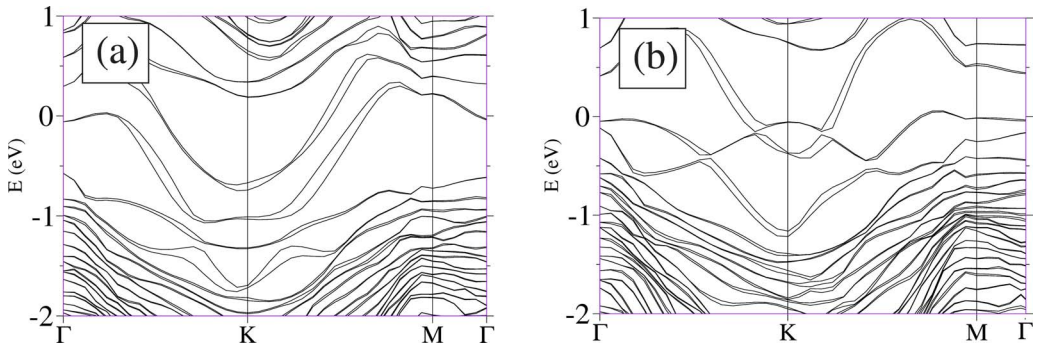

FIG. 8. (Color online) Band structures calculated by using VASP and including the spin-orbit coupling for (a) model p2* and (b) model f2.

pear close to the Fermi level: a dispersive band coming from a silicon dangling bond in the surface and a band derived from the atoms at the step edge (that has a HC structure). These bands are also present for both models. However, while in the case of the f4 structure the step-edge band is completely filled and the dangling-bond band is empty,[18] in the case of the f2 model these two bands cross and the dangling-bond band has a small occupation of ~1/5 electrons closer to the experimental observation.

The population of the different bands can roughly be understood by taking into account the larger electron affinity of gold and the HC structure[39] as compared to other atoms in the surface. The population of the dangling-bond band is thus depleted in favor of the other surface bands. The differences between the f2 and f4 structures are more subtle. These two models only differ in the position of the surface dislocation. Energetically, this structural change has small consequences and both structures are almost degenerate. However, it changes the occupation of the dangling-bond band. In the case of the f2 model, the dislocation involves the gold atoms and some of the silicon atoms of the HC structure. This slightly increases the energy of the bands associated with the HC and, as a consequence, the step-edge band transfers some of its population to the dangling-bond band.

Figure 7 also shows the band structure of the f3 model. The dangling-bond band is missing in this case. This spoils the comparison with experiment. The other two bands (gold and step-edge derived) are very similar to those found for the f2 and f4 models. This is reasonable as it takes into account the similar gold site and structure of the step edge.

Figure 8(b) shows the band structure of the f2 model that is calculated by including the spin-orbit interaction and using the VASP code. The band structure is in excellent agreement with that calculated by using SIESTA. It also confirms the fact that all of the bands close to E_F, with a significant weight in the gold atoms, exhibit a splitting that has its origin in the spin-orbit interaction.

Although the band structure of the model f2 does not exactly reproduce the photoemission results,[3,17,21] particularly the characteristic band fillings mentioned above, it has some clear qualitative similarities with them. We find two bands with similar dispersions, with their minima ~1 and ~0.5 eV below the Fermi energy at the Brillouin-zone boundary. This corresponds very well to the photoemission data. Furthermore, the band with its minima at lower energy shows a notable band splitting near the Fermi energy due to the spin-orbit interaction. This is in good agreement with the experiments. However, the band structure of Fig. 8(b) has two important differences as compared to the photoemission data. First, the dangling-bond band presents an important spin-orbit splitting associated with its appreciable hybridization with gold (see Fig. 7). This splitting is not observed in the experiments. Second, the theoretical band structure has one extra band not seen in photoemission. This band is associated with the HC structure at the step edge and has its minimum at Γ, which is contrary to the case of the other two bands.

We can also compare the predictions for our models with the experimental STM images. In Figs. 9 and 10, we show the simulated STM images at different voltages for the f2 and f4 models. In general, we can say that the comparison with the available experimental data is satisfactory. In agreement with the experimental images,[21,23,24] the most prominent feature is the step edge. Within the terrace, we find signals coming from the row of gold atoms and its neighboring HC structure. The gold chain is seen as a continuous line for occupied states and presents more structure for empty states. For both positive and negative voltages, we can also distinguish a signal coming from the unsaturated silicon dangling bond in the terrace close to the step edge. The step edge and the gold chain could be identified with the two parallel chains reported by Snijders *et al.*[24] In their recent experiment, they observed a strong polarity dependence in the STM images and, in particular, found zigzag structures

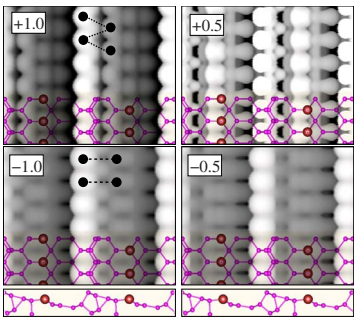

FIG. 9. (Color online) Simulated STM images, calculated by using SIESTA, for model f2. The bias voltage is indicated in volts in each panel. Some features that show a strong polarity dependence are indicated by filled circles.

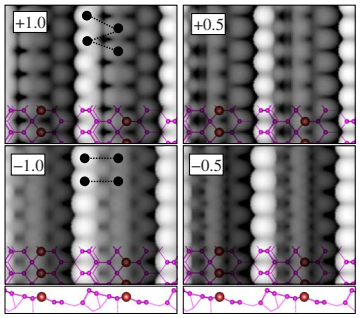

FIG. 10. (Color online) Simulated STM images, calculated by using SIESTA, for model f4. The bias voltage is indicated in volts in each panel. Some features that show a strong polarity dependence are indicated by filled circles.

for empty states and ladder configurations for filled states. In Figs. 9 and 10, we have sketched some possible candidates for this kind of behavior. For f2 (Fig. 9), the ladder structure in filled states could result from the registry of the step edge with respect to the gold atoms. For empty-state images, the step edge becomes slightly more visible and the zigzag geometry could result from the atoms inside the honeycomb chain. In the case of model f4 (Fig. 10), we can identify two entities that change their registries when going from filled to empty states. They are the step edge and the complex formed by Au and the surface dislocation. They show ladder and zigzag configurations, respectively, for filled and empty states, similar to the experiment.

B. Restricted search: Structures based on the π-bonded chain

We first explore two models of the Si(553) stepped silicon surface where the terraces are fully covered by a (2×1) π-bonded chain reconstruction. They correspond to two slightly different arrangements of the π-bonded chain (Fig. 11). Our most stable geometry (model p0) correspond to the so-called negatively tilted π-bonded chain.[70] In low energy electron diffraction experiments of the flat Si(111) surface, the positive-tilt π-bonded chain is usually favored over the negative tilt.[68–70] However, first-principles DFT calculations predict both structure to be very close in energy and there are conflicting claims about which of them is more stable.[71,72]

We now proceed to make all possible substitutions of silicon by gold in the surface bilayer. This gives rise to nine

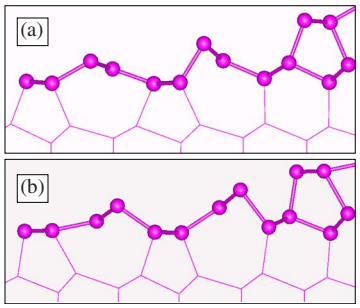

FIG. 11. (Color online) Two possible models of the Si(553) surface based on a π-bonded chain reconstruction of the terraces. Model p in (a) and model p0 in (b).

TABLE II. Relative surface energies of different structures based on a π-bonded chain reconstruction of the terraces of the Si(553) and Si(553)-Au surfaces. Models p and p0 correspond to the clean silicon surface. pX corresponds to the substitution of a gold atom in position X of structure p0. During the relaxation process, several of these structures transform into configurations with a different bonding topology. This change is also indicated. p$X^\star$ refers to pX configurations after the formation of bonds between the step edge and the neighboring π-chain structure. All energies correspond to our most accurate SIESTA calculations.

Name	Configuration	ΔE (meV/Å^2)
p	(1,0,2,12,1,0,2,12,1)	1.82
p0	(1,0,2,21,1,0,2,21,1)	0.00
p1	(3,0,2,21,1,0,2,21,1)	14.92
p2	(1,0,4,21,1,0,2,21,1)→(1,4,2,1,1,0,2,21,1)	4.13
p3	(1,0,2,41,1,0,2,21,1)→(1,2,4,1,1,0,2,21,1)	8.15
p4	(1,0,2,23,1,0,2,21,1)→(1,2,2,3,1,0,2,21,1)	0.00
p5	(1,0,2,21,3,0,2,21,1)→(1,2,0,2,1,3,2,21,1)	7.07
p6	(1,0,2,21,1,0,4,21,1)→(1,2,2,1,1,4,2,1,1)	9.13
p7	(1,0,2,21,1,0,2,41,1)	8.30
p8	(1,0,2,21,1,0,2,23,1)	11.98
p9	(1,0,2,21,1,0,2,21,3)	15.90
p2*		−4.28
p4*		−2.69
p5*		0.38

different models for the Si(553)-Au reconstructions that we name pX, with $X=1$ corresponding to a substitution at the step edge and $X>1$ to a substitution in the terrace. The final energies after accurate SIESTA relaxations (DP level) are listed in Table II. In several cases, the initial structure was not stable and suffers strong modifications during the relaxation. These changes are also summarized in Table II. Model p4, which is illustrated in Fig. 12, is the most stable structure. The π-bonded chain where the gold substitution takes place transforms into a structure similar to the unreconstructed Si(111) surface. This is reasonable because it takes into account the atomic configuration of gold and confirms the tendency of gold to occupy substitutional positions in the middle of the terraces.[3,9,11]

The next most favorable model, p2, is illustrated in Fig. 13. Again the π-bonded chain where the substitution took

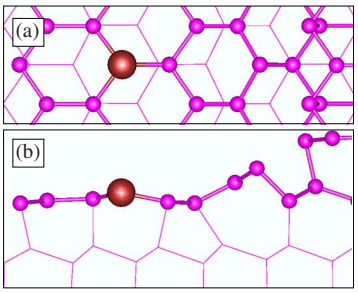

FIG. 12. (Color online) (a) Top and (b) side views of the relaxed structure of the p4 model.

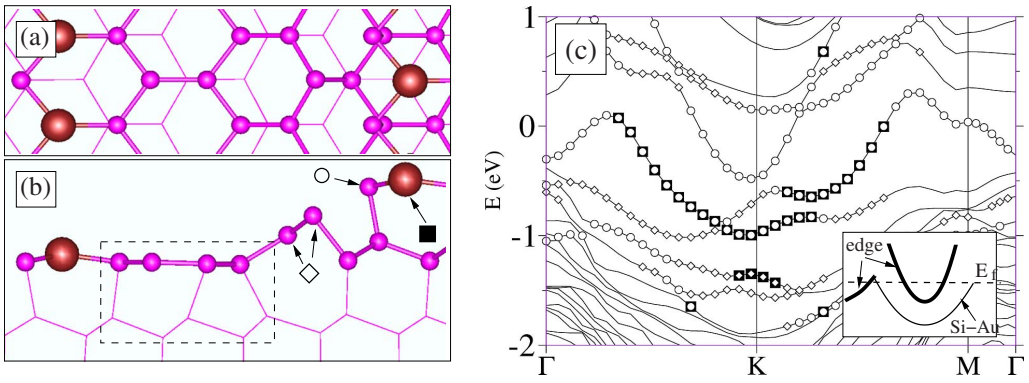

FIG. 13. (Color online) (a) Top and (b) side views of the relaxed structure of the p2 model. (c) Electronic band structure. The symbols highlight those surface bands with an appreciable weight from the surface atoms marked with the same symbols in (b). The inset shows a schematic representation of the most prominent surface bands. The HC structure in the middle of the terrace is indicated by a box.

place has disappeared. However, this time, a configuration reminiscent of the HC structure has formed in the middle of the terrace. This transformation is accompanied by an expansion of the surface bilayer (see the forward movement of the step-edge atoms in Fig. 13).

The band structure calculated for the p2 model, which is shown in Fig. 13(c), presents similar characteristics to the experimental band structure (see the previous section). We can see in Fig. 13(c) that the p2 model features two metallic dispersive bands centered at point K in the zone boundary. One of these bands is associated with the Si-Au bonds between gold and the neighboring silicon atoms in the step edge. It has a considerable gold weight and, therefore, is expected to exhibit a splitting if the spin-orbit coupling is taken into account. The other band, however, is mainly derived from the unsaturated dangling bonds of the silicon atoms at the step edge and presents a smaller filling. As expected, the π-bonded chain structure that remains in the terrace does not give rise to any metallic band.

The electron pocket of the step-edge band around K has an occupation of $\sim 1/4$, which is quite close to that found in the experiment. There is another small electron pocket associated with the step edge at around Γ, which is not observed in the experiment. Thus, we can assign a population of ~ 0.4 to the surface bands with a larger weight in the step-edge atoms. The dispersive band with a mixed silicon-gold character has an occupation of ~ 0.6 electrons. Therefore, the total population associated with the step-edge derived surface bands is 1. This is somewhat surprising if we take into account the fact that the Si atoms at the step edge have, in principle, three electrons to populate these surface bands. However, one of these electrons is transferred to the Au 6s states (which appear several eV below E_F) and the other electron populates states with a large contribution from the HC structure (which does not exhibit any metallic band).

A further investigation of the p2 model reveals that it is a metastable configuration. Performing the relaxations with a more stringent force tolerance of 0.01 eV/Å results in a more stable structure. This structure, which is labeled p2* and illustrated in Fig. 14, exhibits a strong rebonding of the step edge. The π-bonded chain suffers a small translation along the $[\bar{1}10]$ direction in order to saturate the dangling bonds at the step edge. The new position of the atoms of the π-bonded chain seems to be a compromise between creating a surface dislocation and saturating the dangling bonds at the step edge. The band structure, which is shown in Fig. 14(c), is quite similar to that of the p2 model. A quite dispersive surface band, which comes from the Si atoms in the neigh-

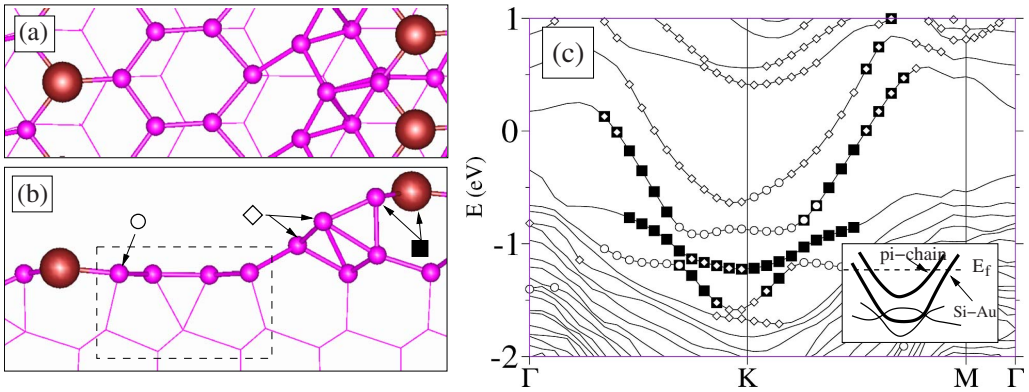

FIG. 14. (Color online) (a) Top and (b) side views of the relaxed structure of the p2* model, which are obtained after the reconstruction of the step edge. (c) Electronic band structure. The symbols indicate those surface bands with an appreciable weight from the surface atoms marked with the same symbols in (b). The inset shows a schematic representation of the most prominent surface bands. The HC structure is highlighted by a box.

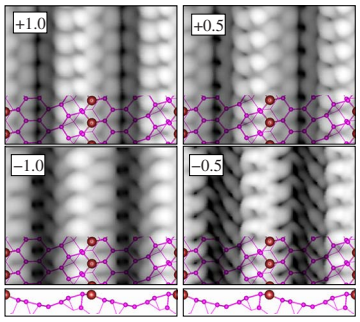

FIG. 15. (Color online) Simulated STM images, calculated by using SIESTA, for model p2⋆. The bias voltage is indicated in volts in each panel.

borhood of the step edge, appears centered at *K*. Another dispersive band with a strong gold weight appears at lower energies. Although the topology of the band structure resembles that observed in the experiment, the filling of the parabolic silicon band is, in this case, close to 0.4, i.e., larger than that observed experimentally. Figure 14(c) also highlights one of the bands associated with the HC structure, which shows a characteristic dispersion.[39]

The band structure of model p2⋆, which is calculated by using VASP and includes the spin-orbit interaction [Fig. 8(a)], shows quite good, although not perfect, agreement with the experiments. As in the case of the f2 model (see above), the dispersive bands suffer a splitting, which is proportional to their weight in the gold atoms. Thus, the splitting is much larger for the dispersive band starting at lower energies. Again, in contradiction to the experimental observations, we also find some degree of splitting for the parabolic band appearing at higher energies, although this splitting is smaller. The overall conclusion from Fig. 8(a) is that the p2⋆ outperforms the f2 model in terms of reproducing the photoemission results.

The simulated STM images for this structural model are shown in Fig. 15. The dependence on polarity seems to be more significant than that for models f2 and f4. The structure of the STM images becomes more complex when going from filled to empty states as several "spots" appear and the identification of zigzag and ladderlike structures becomes quite arbitrary.

Models p4 and p5 exhibit a similar rebonding of the step edge as explained above in the case of p2 and p2*. However, these additional geometries, p4⋆ and p5⋆, are not as stable as p2⋆ (see Table II). Geometry p5⋆ also features the HC structure in the terrace, as can be seen in Fig. 16.

C. Most stable structures: Combined SIESTA and VASP results

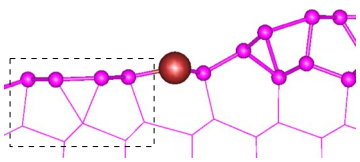

FIG. 16. (Color online) Side view of the p5* model. The HC structure emerges and is highlighted by a box.

TABLE III. Relative surface energies of our most stable models calculated by using both SIESTA and VASP.

	ΔE (meV/Å^2)	
Name	SIESTA	VASP
p2*	4.85	4.93
p4*	6.44	6.54
p5*	9.51	9.13
f1	4.63	4.27
f2	0.17	−0.08
f3	0.42	0.51
f4	0.00	0.00

In Table III, we compare the converged energies of the most stable models found in the previous sections for the Si(553)-Au reconstruction. As discussed in the previous sections, these models have been found (i) by using a systematic search among all possible models based on a flat surface bilayer and eight atoms in the terrace unit cell, and (ii) by the substitution of gold in different positions of a π-bonded reconstruction of the Si(553) terraces. These two classes of models have different numbers of atoms. In order to compare the relative surface energies, we need to define the chemical potential of silicon. Since the surface should be in equilibrium with the bulk, we have chosen the chemical potential to be equal to the total energy of a silicon atom in the bulk. Since the energy differences are quite small, we have decided to perform the calculations of the most stable structure with a different methodology in order to cross-check our results. We have used the plane-wave code VASP for this purpose.[51,52] We can see that there is an excellent agreement between the SIESTA and the VASP results. This was also observed in other similar investigations.[7] Geometries f4 and f2 (see Fig. 6) are the most stable structural models of those found in this extensive structural search. These two models can be considered degenerate within the precision of the calculations.

Models f2 and f4 were already obtained as the most stable ones in a much more restricted structural search.[18] The present calculations confirm that they are certainly among the most stable reconstructions of the Si(553)-Au surface that only involve the topmost bilayer.

IV. CONCLUSIONS

We have presented a comprehensive study of the structure of the Si(553)-Au reconstruction. We have considered reconstructions restricted to the topmost bilayer and studied two possible types: (a) flat surface-bilayer models, where the atoms at the topmost bilayer present different coordinations and different registries with the underlying bulk, and (b) nine different models based on substitutions of silicon by gold in different positions of a π-bonded chain reconstruction of the Si(553) surface.

Although the unreconstructed Si(553) surface has nine inequivalent atomic positions, within the family of the flat surface-bilayer models, we have focused on structures con-

taining only eight atoms (seven silicon and one gold atoms) in the topmost bilayer. In previous investigations, we found that this was crucial to reduce the number of dangling bonds in the final structures and to facilitate the appearance of the so-called honeycomb-chain structure.[9] The honeycomb chain was proposed by us[7,9,11,16,18] and by other authors[3,5] as one of the key ingredients of the reconstructions induced by gold on Si(111) vicinal surfaces, and the results presented here seem to confirm this idea.

We have developed a compact notation that allows us to label and identify all of the structures. This notation is instrumental to the automatic generation of trial geometries and to counting the number of inequivalent structures, i.e., having different bonding topologies. There are several thousands of flat surface-bilayer models with eight inequivalent positions in the topmost bilayer; however, by applying a few physically motivated constraints, we obtained only 210 different models. All of these structures, along with those based on a π-bonded reconstruction of the terraces, have been studied by using first-principles density-functional calculations with the SIESTA code. An iterative procedure, with a step-by-step increase in the accuracy and computational cost of the calculations, was used to allow for the study of this large number of configurations.

The following conclusions can be drawn from our investigation:

(i) Among all of the explored models, the most stable configurations are those that present a honeycomb-chain structure at the step edge. In particular, models f2 and f4 are the most stable (see Fig. 6) with almost degenerate total energies. The structure of both models is very similar, with the sole difference stemming from the relative position of the row of gold atoms and the surface dislocation induced by the presence of the honeycomb chain.

(ii) Within this group of models, the band structure of model f2 shows reasonable agreement with the photoemission measurements.[17,21] It exhibits two one-dimensional bands that share some similarities with the experimental results: both bands have a parabolic dispersion with the band minima at the K point; one of them has a small fractional occupation ($\sim 1/5$). However, both bands present some gold character and, thus, exhibit an appreciable spin-orbit splitting. In the experiment, only *one* band shows a clear splitting.

(iii) The STM images and their dependence on the bias voltage are satisfactorily reproduced by the simulated STM images of models f2 and f4. This is also in agreement with the observations of Ryang *et al.*[41] These authors recently found good agreement between the experimental STM images obtained for the Si(553)-Au surface at low defect concentration and those simulated for a model similar to our f4 structure.

(iv) Of those models based on a π-bonded reconstruction of the Si(553) surface, only p2 and p2* (with p2* being energetically more favorable) present a band structure that is in reasonable agreement with the photoemission measurements. In particular, they exhibit two dispersive one-dimensional bands that are similar to the experimental ones: one of them has a filling close to $1/2$ with a strong gold character and, thus, exhibits a strong spin-orbit splitting; the other one, which comes from the silicon step edge, has a smaller occupation and a quite small spin-orbit splitting that are in good agreement with the photoemission data.

(v) Simulated STM images of the p2* model present a strong polarity dependence. Unfortunately, the patterns appearing are hard to identify with those seen in the experiments.

In summary, it seems that model f2 is a good candidate for the structure of the Si(553)-Au surface. This model presents the lowest total energy and its band structure and simulated STM images are in general agreement with the existing experimental data. The agreement, however, is not perfect. For example, model p2* seems to provide a better comparison with the photoemission data. From a more general perspective, our data clearly point to the importance of the honeycomb-chain structure in stabilizing the surface and, probably, to the presence of a complex rebonding of the step edge, such as that found in the p$X^\star$ models. If this is the case, the structure of the step edge could appreciably depart from that of the initial models considered in the present study. More theoretical and experimental work is therefore necessary to determine if model f2, indeed, corresponds to the high temperature structure of the Si(553)-Au surface reconstruction.

*sampsa.riikonen@iki.fi
†sqbsapod@sc.ehu.es

[1] T. Giamarchi, *Quantum Physics in One Dimension* (Clarendon, Oxford, 2004).
[2] P. Segovia, D. Purdie, M. Hengsberger, and Y. Baer, Nature (London) **402**, 504 (1999).
[3] J. N. Crain, J. L. McChesney, F. Zheng, M. C. Gallagher, P. C. Snijders, M. Bissen, C. Gundelach, S. C. Erwin, and F. J. Himpsel, Phys. Rev. B **69**, 125401 (2004).
[4] R. Losio, K. N. Altmann, and F. J. Himpsel, Phys. Rev. Lett. **85**, 808 (2000).
[5] S. C. Erwin, Phys. Rev. Lett. **91**, 206101 (2003).
[6] I. Matsuda, M. Hengsberger, F. Baumberger, T. Greber, H. W. Yeom, and J. Osterwalder, Phys. Rev. B **68**, 195319 (2003).
[7] S. Riikonen and D. Sánchez-Portal, Phys. Rev. B **71**, 235423 (2005).
[8] R. Losio, K. N. Altmann, A. Kirakosian, J.-L. Lin, D. Y. Petrovykh, and F. J. Himpsel, Phys. Rev. Lett. **86**, 4632 (2001).
[9] D. Sánchez-Portal, J. D. Gale, A. García, and R. M. Martin, Phys. Rev. B **65**, 081401(R) (2002).
[10] I. K. Robinson, P. A. Bennett, and F. J. Himpsel, Phys. Rev. Lett. **88**, 096104 (2002).
[11] D. Sánchez-Portal and R. M. Martin, Surf. Sci. **532-535**, 655 (2003).

[12] J. R. Ahn, H. W. Yeom, H. S. Yoon, and I.-W. Lyo, Phys. Rev. Lett. **91**, 196403 (2003).
[13] D. Sánchez-Portal, S. Riikonen, and R. M. Martin, Phys. Rev. Lett. **93**, 146803 (2004).
[14] H. W. Yeom, J. R. Ahn, H. S. Yoon, I.-W. Lyo, H. Jeong, and S. Jeong, Phys. Rev. B **72**, 035323 (2005).
[15] M. Krawiec, T. Kwapiński, and M. Jalochowski, Phys. Rev. B **73**, 075415 (2006).
[16] S. Riikonen and D. Sánchez-Portal, Phys. Rev. B **76**, 035410 (2007).
[17] J. N. Crain, A. Kirakosian, K. N. Altmann, C. Bromberger, S. C. Erwin, J. L. McChesney, J.-L. Lin, and F. J. Himpsel, Phys. Rev. Lett. **90**, 176805 (2003).
[18] S. Riikonen and D. Sánchez-Portal, Nanotechnology **16**, S218 (2005).
[19] S. K. Ghose, I. K. Robinson, P. A. Bennett, and F. J. Himpsel, Surf. Sci. **581**, 199 (2005).
[20] J. N. Crain and D. T. Pierce, Science **307**, 703 (2005).
[21] J. R. Ahn, P. G. Kang, K. D. Ryang, and H. W. Yeom, Phys. Rev. Lett. **95**, 196402 (2005).
[22] S. Riikonen and D. Sanchez-Portal, Surf. Sci. **600**, 1201 (2006).
[23] J. N. Crain, M. D. Stiles, J. A. Stroscio, and D. T. Pierce, Phys. Rev. Lett. **96**, 156801 (2006).
[24] P. C. Snijders, S. Rogge, and H. H. Weitering, Phys. Rev. Lett. **96**, 076801 (2006).
[25] H. W. Yeom *et al.*, Phys. Rev. Lett. **82**, 4898 (1999).
[26] O. Bunk, G. Falkenberg, J. H. Zeysing, L. Lottermoser, R. L. Johnson, M. Nielsen, F. Berg-Rasmussen, J. Baker, and R. Feidenhansl, Phys. Rev. B **59**, 12228 (1999).
[27] J.-H. Cho, D.-H. Oh, K. S. Kim, and L. Kleinman, Phys. Rev. B **64**, 235302 (2001).
[28] R. H. Miwa and G. P. Srivastava, Surf. Sci. **473**, 123 (2001).
[29] J. R. Ahn, J. H. Byun, H. Koh, E. Rotenberg, S. D. Kevan, and H. W. Yeom, Phys. Rev. Lett. **93**, 106401 (2004).
[30] S. J. Park, H. W. Yeom, S. H. Min, D. H. Park, and I.-W. Lyo, Phys. Rev. Lett. **93**, 106402 (2004).
[31] S. Kurata and T. Yokoyama, Phys. Rev. B **71**, 121306(R) (2005).
[32] J.-H. Cho, J.-Y. Lee, and L. Kleinman, Phys. Rev. B **71**, 081310(R) (2005).
[33] C. González, J. Ortega, and F. Flores, New J. Phys. **7**, 100 (2005).
[34] C. González, F. Flores, and J. Ortega, Phys. Rev. Lett. **96**, 136101 (2006).
[35] H. W. Yeom, Phys. Rev. Lett. **97**, 189701 (2006).
[36] S. Riikonen, A. Ayuela, and D. Sánchez-Portal, Surf. Sci. **600**, 3821 (2006).
[37] J. R. Ahn, J. H. Byun, J. K. Kim, and H. W. Yeom, Phys. Rev. B **75**, 033313 (2007).
[38] I. Barke, F. Zheng, T. K. Rügheimer, and F. J. Himpsel, Phys. Rev. Lett. **97**, 226405 (2006).
[39] S. C. Erwin and H. H. Weitering, Phys. Rev. Lett. **81**, 2296 (1998).
[40] J. R. Ahn, H. W. Yeom, E. S. Cho, and C. Y. Park, Phys. Rev. B **69**, 233311 (2004).
[41] K.-D. Ryang, P. G. Kang, H. W. Yeom, and S. Jeong, Phys. Rev. B **76**, 205325 (2007).
[42] D. Sanchez-Portal, P. Ordejon, E. Artacho, and J. M. Soler, Int. J. Quantum Chem. **65**, 453 (1997).
[43] J. M. Soler, E. Artacho, J. D. Gale, A. García, J. Junquera, P. Ordejón, and D. Sánchez-Portal, J. Phys.: Condens. Matter **14**, 2745 (2002).
[44] J. P. Perdew and A. Zunger, Phys. Rev. B **23**, 5048 (1981).
[45] N. Troullier and J. L. Martins, Phys. Rev. B **43**, 1993 (1991).
[46] H. Häkkinen, M. Moseler, and U. Landman, Phys. Rev. Lett. **89**, 033401 (2002).
[47] E. Artacho, D. Sánchez-Portal, P. Ordejón, A. García, and J. M. Soler, Phys. Status Solidi B **215**, 809 (1999)
[48] J. Junquera, O. Paz, D. Sánchez-Portal, and E. Artacho, Phys. Rev. B **64**, 235111 (2001).
[49] H. J. Monkhorst and J. D. Pack, Phys. Rev. B **13**, 5188 (1976).
[50] J. Tersoff and D. R. Hamann, Phys. Rev. B **31**, 805 (1985).
[51] G. Kresse and J. Hafner, Phys. Rev. B **47**, 558 (1993).
[52] G. Kresse and J. Furthmüller, Phys. Rev. B **54**, 11169 (1996).
[53] S. Kirkpatrick, J. C. D. Gelatt, and M. P. Vecchi, Science **220**, 671 (1983).
[54] V. Černý, J. Optim. Theory Appl. **45**, 41 (1985).
[55] *The Monte Carlo Method in Condensed Matter Physics*, edited by K. Binder (Springer, Berlin, 1992), Vol. 71.
[56] D. M. Deaven and K. M. Ho, Phys. Rev. Lett. **75**, 288 (1995).
[57] K. F. Man, K. S. Tang, and S. Kwong, *Genetic Algorithms* (Springer-Verlag, Berlin, 1999).
[58] V. E. Bazterra, O. Ona, M. C. Caputo, M. B. Ferraro, P. Fuentealba, and J. C. Facelli, Phys. Rev. A **69**, 053202 (2004).
[59] C. V. Ciobanu and C. Predescu, Phys. Rev. B **70**, 085321 (2004).
[60] R. M. Briggs and C. V. Ciobanu, Phys. Rev. B **75**, 195415 (2007).
[61] F. C. Chuang, C. V. Ciobanu, C. Predescu, C. Z. Wang, and K. M. Ho, Surf. Sci. **578**, 183 (2005).
[62] I. L. Garzón, K. Michaelian, M. R. Beltrán, A. Posada-Amarillas, P. Ordejón, E. Artacho, D. Sánchez-Portal, and J. M. Soler, Phys. Rev. Lett. **81**, 1600 (1998).
[63] When the maximum difference between the output and input values of each element of the density matrix in a step of the self-consistent cycle is smaller than DM.Tolerance, a self-consistent solution is assumed to have been achieved. See the manual of the SIESTA code at (http://www.uam.es/siesta).
[64] L. D. Marks and R. Plass, Phys. Rev. Lett. **75**, 2172 (1995).
[65] M. H. Kang and J. Y. Lee, Surf. Sci. **531**, 1 (2003).
[66] J. L. McChesney, J. N. Crain, V. Pérez-Dieste, F. Zheng, M. C. Gallagher, M. Bissen, C. Gundelach, and F. J. Himpsel, Phys. Rev. B **70**, 195430 (2004).
[67] K. C. Pandey, Phys. Rev. Lett. **47**, 1913 (1981).
[68] F. J. Himpsel, P. M. Marcus, R. Tromp, I. P. Batra, M. R. Cook, F. Jona, and H. Liu, Phys. Rev. B **30**, 2257 (1984).
[69] R. M. Tromp, L. Smit, and J. F. van der Veen, Phys. Rev. B **30**, 6235 (1984).
[70] G. Xu, B. Deng, Z. Yu, S. Y. Tong, M. A. VanHove, F. Jona, and I. Zasada, Phys. Rev. B **70**, 045307 (2004).
[71] F. Ancilotto, W. Andreoni, A. Selloni, R. Car, and M. Parrinello, Phys. Rev. Lett. **65**, 3148 (1990).
[72] M. Zitzlsperger, R. Honke, P. Pavone, and U. Schröder, Surf. Sci. **377-379**, 108 (1997).
[73] J. E. Northrup and M. L. Cohen, Phys. Rev. Lett. **49**, 1349 (1982).